Acta Cryst. (1998). A**54**, 74–82

Theoretical Analysis of X-ray Standing Waves and Reflectivity in the Case of a Crystal Containing a Thin Buried Layer

Y. Zheng,* J. C. Boulliard, B. Capelle† and C. Malgrange

Laboratoire de Minéralogie–Cristallographie, Universités Paris VI et Paris VII, CNRS URA009, 4 place Jussieu, 75252 Paris CEDEX 05, France. E-mail: yun_lin.zheng@lmcp.jussieu.fr

(*Received 9 May 1997; accepted 25 July 1997*)

Abstract

The case of a crystal containing a thin buried layer is analysed within the dynamical theory of X-ray diffraction. In this case, the upper thin part of the crystal, above the buried layer, is only shifted with respect to the lower bulk part. The main feature is the phase shift φ for the structure factors between the upper thin part and the lower bulk part. Owing to this phase shift, the backward wavefield, the wavefield with the energy flux directed out of the crystal, is excited in the thin part of the crystal. It is found that only the backward wavefield may be excited within the Bragg total reflection. This gives rise to anomalous transmission of the X-rays in the crystal. When the crystal is tilted across the Bragg angle, the variation of the intensity of X-rays in the buried layer due to the transmission term may be stronger than the one due to the anomalous absorption. Thus, this phenomenon should be taken into account in X-ray standing-wave (XSW) analysis. The excitation of the backward wavefield is also responsible for the appearance of oscillations in the reflectivity profile. The oscillation period is determined by the thickness of the upper thin part. The position and the amplitude of the oscillation directly provide the value of the phase φ. It is thus interesting to simultaneously record the X-ray reflectivity and the XSW measurements when studying the buried layer.

1. Introduction

Since the first works of Batterman (1964, 1969), the technique of X-ray standing waves (XSW) has been widely used for atom location either in the crystal bulk matrix or on the crystal surface [see, for example, the review by Zegenhagen (1993)]. Concerning the atom location in the crystal matrix, the problem of impurities in almost perfect crystals was extensively studied (Golovchenko, Batterman & Brown, 1974; Andersen, Golovchenko & Mair 1976; Materlik & Zegenhagen, 1984; Hertel, Materlik & Zegenhagen, 1985). For the last case, the influence of the disturbed surface layer on the XSW was also analysed by several authors (Kruglov, Shchemelev & Kareva, 1978; Kohn & Kovalchuk, 1981). A general case of a strained epilayer was treated by Authier, Gronkowski & Malgrange (1989) in solving numerically the Takagi–Taupin equations. Recently, the XSW technique has also been applied to the study of ultrathin buried layers, such as a single quantum well (Giannini *et al.*, 1993; Takahasi *et al.*, 1995; Woicik *et al.*, 1995; Boulliard *et al.*, 1997). The case of crystals containing an ultrathin buried layer can be considered as a particular case of an epitaxic system: the epilayer, *i.e.* the upper thin part of the crystal above the buried layer, has the same structure as the bulk and only the buried layer is strained. In this paper, the X-ray dynamical theory is developed for this case. Aspects on the XSW and X-ray reflectivity will be analysed and the connection between the XSW and X-ray reflectivity measurements discussed.

High-resolution X-ray reflectivity is commonly used for analysing epitaxic thin films. For a buried layer, the reflectivity profiles also provide characteristics of both the upper thin part of the crystal and the buried layer.

The presence of the upper thin part of the crystal strongly influences the X-ray propagation, as will be explained in this paper. It is worth pointing out the similarities and differences between an epitaxic thin film and a buried layer. Whenever the thin-film Bragg angle is very different from that of the substrate, the reflectivity allows one to determine the film lattice parameter from the film peak position and the film thickness from the weak oscillation period. When the Bragg angles of the film and the substrate are close, strong interactions occur between the X-rays in the film and in the substrate. Thus, a dynamical analysis is necessary. In the case of a strained thin film, the Takagi–Taupin equations should be numerically solved to understand the X-ray propagation and to extract the strain parameters (Gronkowski, 1991; Bensoussan, Malgrange & Sauvage-Simkin, 1987; Vandenberg, Hamm & Chu, 1994). In the present study, the two parts of the crystal, above and below the buried layer, have the same structure. Strong dynamical effects occur in the diffraction process. One cannot separate in the Bragg reflection the contributions from the thin part and the bulk. This phenomenon is detailed below.

† Also at LURE, CNRS-MEN-CEA, Bâtiment 209D, 91405 Orsay, France.

ISSN 0108-7673

In this paper, we will firstly recall features of the X-ray dynamical theory in the Bragg case necessary for the present study (§2). The analytical solutions of X-ray waves will be given for crystals containing an ultrathin buried layer (§3). Main characteristics in the X-ray propagation, *i.e.* excitation of the backward wavefield (§4.1) and penetration of the X-rays into the crystal (§4.2), will be discussed. Direct consequences of the analysis of the XSW and X-ray reflectivity measurements will be pointed out (§§4.3, 4.4, 4.5).

2. X-ray dynamical theory

In this paper, only σ polarization will be considered. The notation and convention used follow Authier (1961, 1986), except for the reflection vector **h** (Fig. 1). After Authier's notation, the unit vector **n**, normal to the crystal surface, points into the crystal. $\mathbf{K}_0^{(a)}$ and $\mathbf{K}_\mathbf{h}^{(a)}$ represent the incident and reflected wave vectors in vacuum respectively, while $\mathbf{K}_0$ and $\mathbf{K}_\mathbf{h}$ are the incident and reflected wave vectors in the crystal, respectively. $\gamma_0 = \cos(\mathbf{n}, \mathbf{K}_0)$ with $(\mathbf{n}, \mathbf{K}_0)$ the angle between **n** and $\mathbf{K}_0$, while $\gamma_\mathbf{h} = \cos(\mathbf{n}, \mathbf{K}_\mathbf{h})$ with $(\mathbf{n}, \mathbf{K}_\mathbf{h})$ the angle between **n** and $\mathbf{K}_\mathbf{h}$. In the present notation, γ_0 is positive and $\gamma_\mathbf{h}$ negative. For the purpose of XSW, it is convenient to point the vector **h** out of the crystal. **h** is thus defined as $\mathbf{K}_\mathbf{h} = \mathbf{K}_0 + \mathbf{h}$, with the opposite sign with respect to Authier's notation.

In the two-wave approximation, X-ray wavefields in a perfect crystal, *i.e.* the dielectric displacement $D(\mathbf{r})$, can be written as Bloch waves:

$$D(\mathbf{r}) = D_0 \exp(-i2\pi\mathbf{K}_0 \cdot \mathbf{r}) + D_\mathbf{h} \exp[-i2\pi(\mathbf{K}_0 + \mathbf{h}) \cdot \mathbf{r}]$$
$$= D_0 \exp(-i2\pi\mathbf{K}_0 \cdot \mathbf{r})[1 + \xi \exp(-i2\pi\mathbf{h} \cdot \mathbf{r})], \quad (1)$$

where ξ is the complex amplitude ratio $D_\mathbf{h}/D_0$. The wavefields are solutions of

$$[K_0^2 - k^2(1 + \chi_0)]D_0 - k^2\chi_{\bar{\mathbf{h}}}D_\mathbf{h} = 0$$
$$k^2\chi_\mathbf{h}D_0 - [K_\mathbf{h}^2 - k^2(1 + \chi_0)]D_\mathbf{h} = 0. \quad (2)$$

Here k is the magnitude of the incident wave vector $\mathbf{K}_0^{(a)}$ in vacuum. χ_0, $\chi_\mathbf{h}$ and $\chi_{\bar{\mathbf{h}}}$ are the **o**, **h** and $-\mathbf{h}$ Fourier components of the dielectric susceptibility, respectively. They are proportional to the structure factors F_0, $F_\mathbf{h}$ and $F_{\bar{\mathbf{h}}}$, respectively. The continuity of the tangential component of the wave vectors along the crystal surface provides two solutions:

$$\mathbf{K}_0 = \mathbf{K}_0^{(a)} + (k\chi_0/2\gamma_0)\mathbf{n} - (1/2\Lambda)[\eta \pm (\eta^2 - 1)^{1/2}]\mathbf{n}. \quad (3)$$

The second term describes the refraction effect. The linear absorption is contained in the imaginary part of $k\chi_0/2\gamma_0$. $\Lambda = (\gamma_0|\gamma_\mathbf{h}|)^{1/2}/[k(\chi_\mathbf{h}\chi_{\bar{\mathbf{h}}})^{1/2}]$ is the extinction distance. The deviation parameter η is defined by

$$\eta = \frac{\sin 2\theta[\Delta\theta - \Delta\theta_0]}{(\chi_\mathbf{h}\chi_{\bar{\mathbf{h}}})^{1/2}(|\gamma_\mathbf{h}|/\gamma_0)^{1/2}}, \quad (4)$$

where $\Delta\theta$ is the departure from the exact Bragg angle θ_B for the incident wave and $\Delta\theta_0 = -\chi_0(1 - \gamma_\mathbf{h}/\gamma_0)/2\sin 2\theta$. The Bragg total reflection range in the case of a non-absorbing crystal corresponds to $|\eta| \leq 1$.

The amplitude ratio ξ of each wavefield, correponding to each solution of (3), is given by

$$\xi = -[(\chi_\mathbf{h}\chi_{\bar{\mathbf{h}}})^{1/2}/\chi_{\bar{\mathbf{h}}}](\gamma_0/|\gamma_\mathbf{h}|)^{1/2}[\eta \pm (\eta^2 - 1)^{1/2}]. \quad (5)$$

Let us call 'the forward wavefield' the one that propagates in a thick crystal because the energy flux associated is directed into the crystal. We will call 'the backward wavefield' the second wavefield because the energy flux is directed out of the crystal. To distinguish which solution for equations (3) and (5) corresponds to the forward wavefield, we will analyse the possible choice for the signs. Outside the Bragg reflection ($|\eta| > 1$), ξ for the forward wavefield should decrease for increasing η. Thus, in equations (3) and (5), one must choose the + sign for $\eta_r < -1$ and the − sign for $\eta_r > +1$, where η_r is the real part of η. Within the Bragg total reflection range ($|\eta| \leq 1$), only the evanescent wave exists in a thick crystal. The imaginary part of the wave vector [equation (3)] of the forward wavefield must be negative.

For the sake of simplicity, let us define a sign function $\varepsilon(\eta)$ so that $[\eta + \varepsilon(\eta)(\eta^2 - 1)^{1/2}]$ corresponds to the solution for the forward wavefield. It means that

$$\varepsilon(\eta) = \begin{cases} -\text{sign}(\eta_r) & \text{for } |\eta| > 1 \\ \text{sign}\{\text{Im}[(\eta^2 - 1)^{1/2}/\Lambda]\} & \text{for } |\eta| \leq 1, \end{cases}$$

where Im[x] is the imaginary part of x. Thus, we denote (+) all the components of the forward wavefield, namely

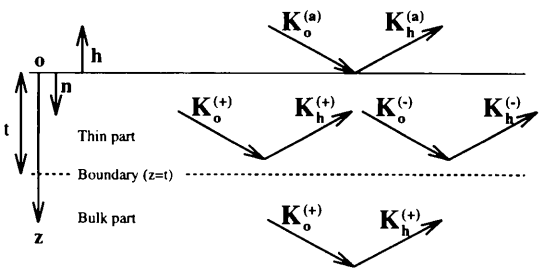

Fig. 1. Notation and convention used. The unit vector **n** is normal to the crystal surface and the *oz* axis points into the crystal. The reflecting vector **h** points out of the crystal. The thin buried layer in the crystal is assimilated with a boundary at a depth $z = t$ for the X-ray propagation. $\mathbf{K}_0^{(a)}$ and $\mathbf{K}_\mathbf{h}^{(a)}$ represent, respectively, the incident and reflected wave vectors in vacuum. $\mathbf{K}_0^{(+)}$ and $\mathbf{K}_\mathbf{h}^{(-)}$ represent, respectively, the incident and reflected wave vectors in the bulk part of the crystal. Additional wave vectors in the thin part of the crystal $\mathbf{K}_0^{(-)}$ and $\mathbf{K}_\mathbf{h}^{(-)}$ represent, respectively, the incident and reflected wave vectors of the backward wavefield (*cf.* §2).

the incident wave vector as $\mathbf{K}_0^{(+)}$ and the amplitude ratio as $\xi^{(+)}$:

$$\mathbf{K}_0^{(+)} = \mathbf{K}_0^{(a)} + (k\chi_0/2\gamma_0)\mathbf{n} - (1/2\Lambda)[\eta + \varepsilon(\eta^2 - 1)^{1/2}]\mathbf{n} \tag{6}$$

and

$$\xi^{(+)} = -[(\chi_\mathbf{h}\chi_{\bar{\mathbf{h}}})^{1/2}/\chi_{\bar{\mathbf{h}}}](\gamma_0/|\gamma_\mathbf{h}|)^{1/2}[\eta + \varepsilon(\eta^2 - 1)^{1/2}]. \tag{7}$$

The backward wavefield corresponds to $\mathbf{K}_0^{(-)}$ and $\xi^{(-)}$, obtained by replacing ε by $-\varepsilon$. The energy flux of the backward wavefield is directed out of the crystal in the range outside the Bragg total reflection. The amplitude of the backward wavefield increases exponentially with the depth within the Bragg total reflection range.

One important feature of a wavefield is the positions of the XSW antinodes. The antinode positions are determined by the phase of the reflected wave with respect to the incident one. For the present case, the phases of the XSW associated with both wavefields are equal to the phases of $\xi^{(+)}$ and $\xi^{(-)}$, respectively. Since the structure factor is generally complex in absorbing crystals, a physical insight of the phase variation can be obtained with the non-absorbing case. When taking the origin of the reflecting planes at the maximum of the electronic density in the non-absorbing case, the structure factor $F_\mathbf{h}$ is real and its phase is equal to zero. Thus, from (7) and for the Bragg total reflection range ($|\eta| \leq 1$), the phase Ψ of $\xi^{(+)}$ can be written as

$$\begin{aligned}\Psi &= \text{phase of } [\eta + \varepsilon(\eta^2 - 1)^{1/2}] \\ &= \text{phase of } [\eta + i(1 - \eta^2)^{1/2}] \\ &= \arccos(\eta).\end{aligned} \tag{8}$$

The phase of $\xi^{(-)}$ is simply equal to $-\Psi$. When η varies from -1 to 1, Ψ drops from π to 0. It means that, when the crystal is tilted across the Bragg reflection by increasing angles, the XSW antinodes of the forward wavefield move inwards from between the reflecting planes to the reflecting planes, as occurs in a thick crystal (Bedzyk & Materlik, 1985; Authier, 1986). For the backward wavefield, the XSW antinodes move outwards from between the reflecting planes to the reflecting planes.

A general solution of the set of equations (2) is given by the sum of the forward and backward wavefields.

3. Solution in the case of a crystal containing a thin buried layer

We assume that the buried layer induces only a displacement of the atoms and thus a phase shift for the structure factors. It means that it only induces a supplementary phase shift φ between the reflected and incident waves. This is typically the model for a stacking fault. It can be extended to the case of a thin buried layer where the change in the amplitudes of the waves can be neglected. Thus, the buried layer is simply assimilated to a boundary for the X-ray propagation. One may write $\varphi = 2\pi\mathbf{h}\cdot\Delta\mathbf{r}$, where $\Delta\mathbf{r}$ is the displacement due to the buried layer. Taking the bulk as the reference, the changes for the components in the thin part should be made:

$$\chi_\mathbf{h} \rightarrow \chi_\mathbf{h}\exp(i\varphi), \quad \chi_{\bar{\mathbf{h}}} \rightarrow \chi_{\bar{\mathbf{h}}}\exp(-i\varphi)$$

and from (5):

$$\xi \rightarrow \xi\exp(i\varphi).$$

The waves in the vacuum $D^{(a)}(\mathbf{r})$, in the upper thin part $D^{(t)}(\mathbf{r})$ and in the bulk $D^{(b)}(\mathbf{r})$ may be expressed as:

for $z \leq 0$:

$$\begin{aligned}D^{(a)}(\mathbf{r}) &= D_0^{(a)}\exp[-i2\pi\mathbf{K}_0^{(a)}\cdot\mathbf{r}] \\ &\quad + D_\mathbf{h}^{(a)}\exp[-i2\pi(\mathbf{K}_0^{(a)} + \mathbf{h})\cdot\mathbf{r}]\end{aligned}$$

for $0 \leq z \leq t$:

$$\begin{aligned}D^{(t)}(\mathbf{r}) &= D_0^{(+)}\exp[-i2\pi\mathbf{K}_0^{(+)}\cdot\mathbf{r}] \\ &\quad \times [1 + \xi^{(+)}\exp(i\varphi)\exp(-i2\pi\mathbf{h}\cdot\mathbf{r})] \\ &\quad + D_0^{(-)}\exp[-i2\pi\mathbf{K}_0^{(-)}\cdot\mathbf{r}] \\ &\quad \times [1 + \xi^{(-)}\exp(i\varphi)\exp(-i2\pi\mathbf{h}\cdot\mathbf{r})]\end{aligned}$$

for $z \geq t$:

$$\begin{aligned}D^{(b)}(\mathbf{r}) &= D_0^{(b)}\exp[-i2\pi\mathbf{K}_0^{(+)}\cdot\mathbf{r}] \\ &\quad \times [1 + \xi^{(+)}\exp(-i2\pi\mathbf{h}\cdot\mathbf{r})].\end{aligned} \tag{9}$$

The continuity of the tangential component of the wave vectors along the surface ($z = 0$) and the boundary ($z = t$) is fulfilled with the definition of $\mathbf{K}_0^{(+)}$ and $\mathbf{K}_0^{(-)}$. Thus further boundary conditions concern the continuity of the electric displacements:

at $z = 0$:

$$\begin{aligned}D_0^{(a)} &= D_0^{(+)} + D_0^{(-)} \\ D_\mathbf{h}^{(a)} &= \exp(i\varphi)[D_0^{(+)}\xi^{(+)} + D_0^{(-)}\xi^{(-)}]\end{aligned}$$

at $z = t$:

$$\begin{aligned}D_0^{(b)} &= D_0^{(+)} + D_0^{(-)}\exp[-i2\pi t(\mathbf{K}_0^{(-)} - \mathbf{K}_0^{(+)})\cdot\mathbf{n}] \\ D_0^{(b)}\xi^{(+)} &= \exp(i\varphi)\{D_0^{(+)}\xi^{(+)} + D_0^{(-)}\xi^{(-)} \\ &\quad \times \exp[-i2\pi t(\mathbf{K}_0^{(-)} - \mathbf{K}_0^{(+)})\cdot\mathbf{n}]\}.\end{aligned} \tag{10}$$

From the above equations (10), one obtains

$$\begin{aligned}D_0^{(+)}/D_0^{(a)} &= 1/\{1 + C\exp[i2\pi(t/\Lambda)\varepsilon(\eta^2 - 1)^{1/2}]\} \\ D_0^{(-)}/D_0^{(a)} &= \{C\exp[i2\pi(t/\Lambda)\varepsilon(\eta^2 - 1)^{1/2}]\} \\ &\quad \times \{1 + C\exp[i2\pi(t/\Lambda)\varepsilon(\eta^2 - 1)^{1/2}]\}^{-1} \\ D_0^{(b)}/D_0^{(a)} &= (1 + C)/\{1 + C\exp[i2\pi(t/\Lambda)\varepsilon(\eta^2 - 1)^{1/2}]\},\end{aligned} \tag{11}$$

where the coefficient C is

$$C = -[1 - \exp(i\varphi)]/\{1 - \exp(i\varphi)[\eta - \varepsilon(\eta^2 - 1)^{1/2}]^2\}. \quad (12)$$

4. Analysis and discussion

We will now study the excitation of the backward wavefield in the upper thin part of the crystal and analyse the consequences in the X-ray propagation. We will first treat the non-absorbing case which can be analytically detailed. Then the difference between the absorbing and non-absorbing cases will be pointed out.

4.1. *Backward wavefield in the thin part of the crystal*

Let us first define a parameter which characterizes the excitation of the backward wavefield as a function of the phase shift φ. One significant parameter is the ratio between the D_0 amplitudes of the backward and forward wavefields at the boundary ($z = t$). It can be easily shown that the coefficient C defined in equation (12) corresponds to this parameter:

$$\{D_0^{(-)} \exp[-i2\pi t\mathbf{K}_0^{(-)} \cdot \mathbf{n}]\}/\{D_0^{(+)} \exp[-i2\pi t\mathbf{K}_0^{(+)} \cdot \mathbf{n}]\} = C.$$

4.1.1. *Non-absorbing case.* For the Bragg total reflection range ($|\eta| \leq 1$), it is deduced from (8) that

$$[\eta - \varepsilon(\eta^2 - 1)^{1/2}] = [\eta - i(1 - \eta^2)^{1/2}] = \exp(-i\Psi).$$

Thus, the expression (12) for C for $|\eta| \leq 1$ is simplified as:

$$C = \exp(i\Psi)\sin(\varphi/2)/\sin(\Psi - \varphi/2). \quad (13)$$

The parameter C becomes infinite for $\Psi = \varphi/2$, *i.e.* $\eta = \cos(\varphi/2)$. Since C is the ratio between the D_0 amplitudes of the backward and forward wavefields at $z = t$, only the backward wavefield is excited in the thin part of the crystal. This effect can be geometrically explained (Fig. 2). There is a full transfer between the forward wavefield in the bulk and the backward one in the thin part, when they are exactly in phase, *i.e.* the antinodes of their standing waves are at the same position (modulus the reflecting plane spacing). This gives rise to an anomalous transmission of the X-rays as will be discussed in the next section. The transfer is minimal for $\Psi = \varphi/2 \pm \pi/2$, *i.e.* $\eta = \mp\sin(\varphi/2)$. The antinodes of the standing waves, associated with the backward wavefield in the thin part and with the forward wavefield in the bulk, are located at a distance of one half of the reflecting plane spacing. Thus, the excitation of the backward wavefield is minimized [$|C| = |\sin(\varphi/2)|$]. There is no condition for the complete extinction of the backward wavefield.

4.1.2. *Absorbing case.* The main difference is that C does not become infinite. There is no longer full transfer between the forward wavefield in the bulk and the backward one. An example for GaAs(001) with a boundary at a depth of 1000 Å is shown in Fig. 3. Values of $|C|$ are drawn as a function of η_r for $\varphi = \pi/4$ and $\pi/2$. $|C|$ becomes maximum when $\eta_r = \cos(\varphi/2)$. The maximum value beomes infinite for a non-absorbing crystal.

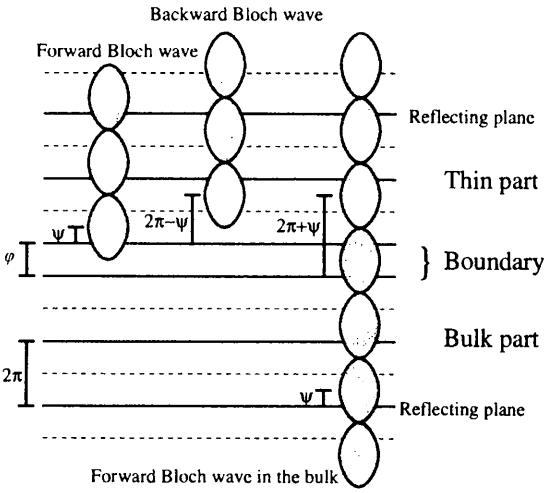

Fig. 2. Full transfer between the forward wavefield in the bulk and the backward one in the thin part. The positions of the reflecting planes are symbolized by solid lines and the middle by dashed lines. The spacing between reflecting planes is expressed in terms of phase as 2π. The full transfer occurs for $\varphi + 2\pi - \Psi = 2\pi + \Psi$ when the backward wavefield and the forward one in the bulk are in phase; *i.e.* the antinodes of their standing waves are at the same position (modulus the reflecting plane spacing).

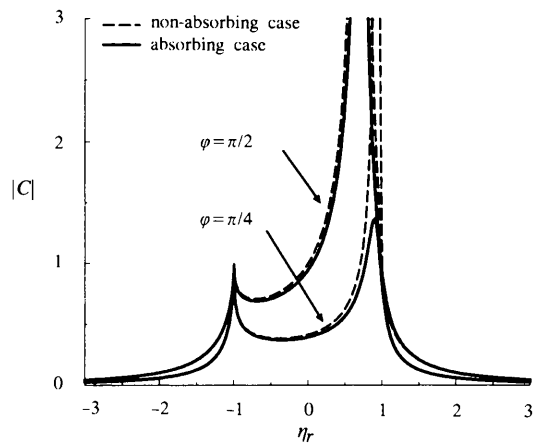

Fig. 3. Absolute ratio $|C|$ of the D_0 amplitudes between the backward and forward wavefields at the crystal boundary. Curves are for GaAs(001) with a boundary at a depth $t = 1000$ Å, $\lambda = 1.6$ Å and 004 reflection. Curves are drawn for $\varphi = \pi/4$ and $\pi/2$. For the non-absorbing case, the shape of the curves depends on the ratio t/Λ only.

4.2. *X-ray penetration into the crystal*

In the Bragg total reflection range, the amplitude of the backward wavefield increases exponentially as a function of the depth. For the non-absorbing case, the backward wavefield only is excited when $\eta = \cos(\varphi/2)$. In the last case, the intensity of the X-rays increases from the surface up to $z = t$ and decreases in the bulk. It may seem surprising that the intensity of the X-rays becomes firstly larger than the intensity of the incident beam. In fact, only the intensity of the non-propagating X-ray field becomes larger than the incident one and not the propagated energy, as the energy does not propagate into the crystal during the total reflection. Let us calculate the intensities of the X-rays, normalized with respect to the one of the incident wave, along the incident direction $\mathbf{K}_0$ into the crystal:

for $0 \le z \le t$:

$$\begin{aligned} I_0^{(t)} &= |[D_0^{(+)}/D_0^{(a)}]\exp[-i2\pi\mathbf{K}_0^{(+)}\cdot\mathbf{r}] \\ &\quad + [D_0^{(-)}/D_0^{(a)}]\exp[-i2\pi\mathbf{K}_0^{(-)}\cdot\mathbf{r}]|^2 \\ &= |\exp[-i2\pi\mathbf{K}_0^{(+)}\cdot\mathbf{r}]|^2 \\ &\quad \times \left|\left(1 + C\exp\{i2\pi[(t-z)/\Lambda]\varepsilon(\eta^2-1)^{1/2}\}\right)\right. \\ &\quad \left.\times\{1 + C\exp[i2\pi(t/\Lambda)\varepsilon(\eta^2-1)^{1/2}]\}^{-1}\right|^2 \end{aligned}$$

for $z \ge t$:

$$\begin{aligned} I_0^{(b)} &= |[D_0^{(b)}/D_0^{(a)}]\exp[-i2\pi\mathbf{K}_0^{(+)}\cdot\mathbf{r}]|^2 \\ &= |\exp[-i2\pi\mathbf{K}_0^{(+)}\cdot\mathbf{r}]|^2 \\ &\quad \times |(1+C)/\{1 + C\exp[i2\pi(t/\Lambda)\varepsilon(\eta^2-1)^{1/2}]\}|^2. \end{aligned} \tag{14}$$

The first term in the above expressions, $|\exp[-i2\pi\mathbf{K}_0^{(+)}\cdot\mathbf{r}]|^2$, is equal to the usual anomalous absorption in a thick crystal. The second term which appears because of the existence of the backward wavefield will be called the transmission term.

4.2.1. *Non-absorbing case.* Within the total reflection range, the usual anomalous absorption is given by $|\exp[-i2\pi\mathbf{K}_0^{(+)}\cdot\mathbf{r}]|^2 = \exp[-2\pi(z/\Lambda)(1-\eta^2)^{1/2}]$. For a given value of φ, one may consider the two extreme cases where the excitation of the backward wavefield is either maximum or minimum. At the maximal excitation $[\eta = \cos(\varphi/2)]$, $|C|$ tends to infinity and the intensity varies as

$$\begin{aligned} I_0^{(t)} &= \exp[-2\pi(z/\Lambda)(1-\eta^2)^{1/2}] \\ &\quad \times \exp[+4\pi(z/\Lambda)(1-\eta^2)^{1/2}] \\ &= \exp[+2\pi(z/\Lambda)(1-\eta^2)^{1/2}] \\ I_0^{(b)} &= \exp[-2\pi(z/\Lambda)(1-\eta^2)^{1/2}] \\ &\quad \times \exp[+4\pi(t/\Lambda)(1-\eta^2)^{1/2}] \\ &= \exp\{-2\pi[(z-2t)/\Lambda](1-\eta^2)^{1/2}\}. \end{aligned}$$

As expected, the intensity exponentially increases until $z = t$ and then decreases in the bulk (Fig. 4). At the minimal excitation, similar considerations from equations (14) indicate that the intensity varies as for a single perfect crystal, with a slightly stronger attenuation (Fig. 4). For a given φ, the intensity variation for other values of η are between the two extreme cases (Fig. 4).

4.2.2. *Absorbing case.* Within the total reflection range, the above considerations also apply. Indeed the penetration depth for either the evanescent wave or the exponential wave depends on the extinction distance Λ which remains the same in the two cases.

4.3. *X-ray standing waves at the boundary of the crystal*

In the case of a single perfect crystal, the intensity of the X-ray standing waves on the surface is given by

$$|D(\mathbf{r})|^2_{\text{p.c.}} = |D_0^{(a)}|^2|1 + \xi^{(+)}\exp(-i2\pi\mathbf{h}\cdot\mathbf{r})|^2, \tag{15}$$

where 'p.c.' means the perfect crystal. When one considers the intensity of the X-ray standing waves at the boundary of the crystal, $|D_0^{(a)}|^2$ in the above expression should be replaced by the intensity of the incident beam at the boundary. As a result, (15) has to be multiplied by the normalized intensity at the boundary $I_0^{(t)}(z=t) = I_0^{(b)}(z=t)$ given by (14). As indicated in the previous section, this factor is made of two terms: (*a*) the correction due to the anomalous absorption which exists even in the case of a perfect crystal ($\varphi = 0$); (*b*) the correction for the transmission of the X-rays through the thin part $T(\eta)$. From (5), it can be seen that the anomalous-absorption term is

$$|\exp[-i2\pi t\mathbf{K}_0^{(+)}\cdot\mathbf{n}]|^2 = \exp(-t/z_o) \tag{16}$$

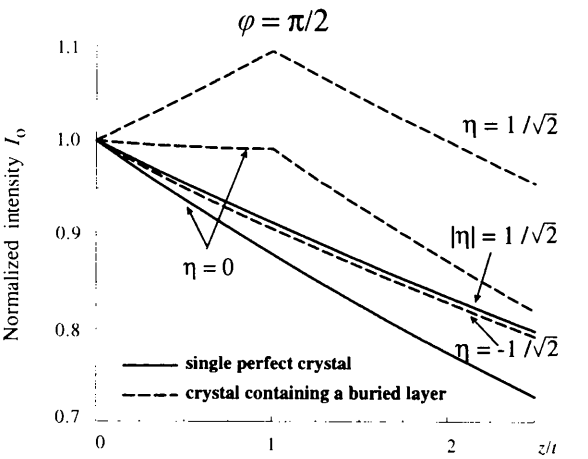

Fig. 4. Normalized intensity I_0 of the X-rays into the crystal. Curves are for the non-absorbing case of GaAs(001) with a boundary at a depth $t = 1000$ Å, $\varphi = \pi/2$, $\lambda = 1.6$ Å and 004 reflection. Curves for a single perfect crystal are drawn for comparison. The exponential behaviour as a function of the depth is not easily visible for this range of thicknesses.

with z_o the usual penetration depth:

$$(1/z_o) = 2\pi \,\mathrm{Im}\{-(k\chi_0/\gamma_0) + (1/\Lambda)[\eta + \varepsilon(\eta^2 - 1)^{1/2}]\}.$$

The transmission term is given by

$$T(\eta) = |(1 + C)/\{1 + C\exp[i2\pi(t/\Lambda)\varepsilon(\eta^2 - 1)^{1/2}]\}|^2. \tag{17}$$

The intensity of the X-ray standing waves at the boundary is thus determined by

$$|D(\mathbf{r})|^2 = T(\eta)\exp(-t/z_o)|D(\mathbf{r})|^2_{\mathrm{p.c.}}. \tag{18}$$

The variation of $T(\eta)$ is illustrated in Fig. 5 for different values of φ and the anomalous-absorption term is also drawn for comparison. As indicated in the previous section, for a given value of φ, the transmission is maximum at $\eta_r = \cos(\varphi/2)$. For this value, the transmission is about $\exp(2t/z_o)$, so that the total correction is $\exp(t/z_o)$. Depending on the value of φ, the transmission term is roughly of the same order as the anomalous absorption one, with a maximal effect for $\varphi = \pi$. However, the variation of the two correction terms as a function of η is different. Thus they must be taken into account together for the XSW analysis when t is not small in comparison with the extinction distance Λ.

Let us establish a qualitative criterion concerning this last point. With regard to the high precision of the XSW measurements, one can roughly estimate that the transmission and the anomalous absorption are not negligible when $2\pi t/\Lambda > 0.05$. For instance, for $2\pi t/\Lambda = 0.05$, the maximal correction in the XSW intensity at the buried layer depth is 0.95 for the anomalous absorption and 1.10 for the transmission term when $\varphi = \pi$. Table 1 lists such minimal thicknesses $t = 0.05\Lambda/2\pi$ for Si, Ge, GaAs and CdTe crystals. It appears that the corrections should be added for t larger than several hundred Å. The thickness t should be understood as the effective thickness which is larger than the nominal one for inclined Bragg reflections in XSW experiences (Golovchenko, Patel, Kaplan, Cowan & Bedzyk, 1982; Taccoen, Malgrange, Zheng, Boulliard & Capelle, 1994). For an inclined symmetric reflection, for instance, the effective thickness is increased from the nominal one by the factor $1/\cos(-\mathbf{n}, \mathbf{h})$ with $(-\mathbf{n}, \mathbf{h})$ the angle between the crystal surface normal vector $-\mathbf{n}$ and the reflecting vector $\mathbf{h}$.

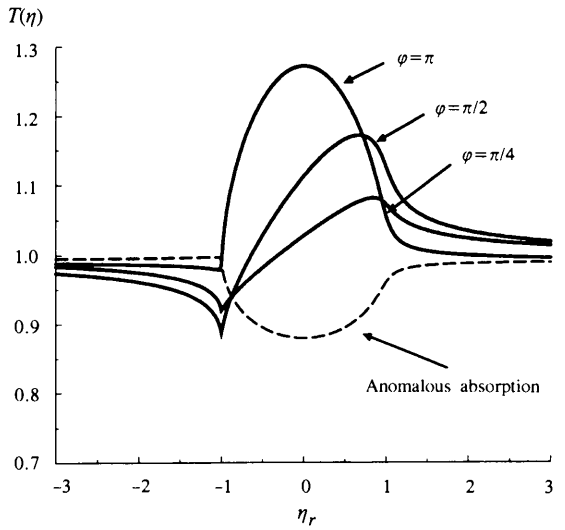

Fig. 5. Transmission $T(\eta)$ of the X-rays through the thin part of the crystal for $\varphi = \pi/4$, $\pi/2$ and π. Curves are for the absorbing case of GaAs(001) with a boundary at a depth $t = 1000$ Å, $\lambda = 1.6$ Å and 004 reflection. The anomalous-absorption term is drawn for comparison.

Table 1. *Comparison of the thicknesses t ($= 0.05\Lambda/2\pi$) (Å) between Si, Ge, GaAs and CdTe for 004, 022 and 111 reflections at $\lambda = 1.6$ Å*

Reflection	Si	Ge	GaAs	CdTe
004	894	366	392	271
022	531	220	228	168
111	375	165	166	126

4.4. *X-ray waves on the surface of the crystal and reflectivity*

Besides a strong dynamical effect within the Bragg reflection range, the excitation of the backward wavefield is also responsible for the appearance of long-period weak oscillations far from the Bragg reflection. From (10), the amplitude ratio $\xi^{(a)}$ $(= D_{\mathbf{h}}^{(a)}/D_{\mathbf{0}}^{(a)})$ in vacuum is obtained:

$$\begin{aligned}\xi^{(a)} = \xi^{(+)}\exp(i\varphi)\{1 + [\eta - \varepsilon(\eta^2 - 1)^{1/2}]^2 \\ \times C\exp[i2\pi(t/\Lambda)\varepsilon(\eta^2 - 1)^{1/2}]\} \\ \times \{1 + C\exp[i2\pi(t/\Lambda)\varepsilon(\eta^2 - 1)^{1/2}]\}^{-1}.\end{aligned} \tag{19}$$

The reflectivity R is related to the absolute value of $\xi^{(a)}$. Let us call $R_{\mathrm{p.c.}}$ the reflectivity in the case of a single perfect crystal and R_{osc} the oscillating part for the reflectivity. The total reflectivity R is

$$R = R_{\mathrm{osc}}R_{\mathrm{p.c.}} \tag{20}$$

with

$$R_{\mathrm{p.c.}} = |\gamma_{\mathbf{h}}/\gamma_{\mathbf{0}}||\xi^{(+)}|^2 \quad \text{and} \quad R_{\mathrm{osc}} = |\xi^{(a)}/\xi^{(+)}|^2.$$

4.4.1. *Non-absorbing case.* When $|\eta| \gg 1$, $[\eta - \varepsilon(\eta^2 - 1)^{1/2}] \approx 2\eta$ and $C \approx -i\exp(-i\varphi/2) \times \sin(\varphi/2)/(2\eta^2)$, $\xi^{(a)}$ can be approximated by

$$\begin{aligned}\xi^{(a)} \approx \xi^{(+)}\exp(i\varphi)\{1 + 2\sin(\varphi/2) \\ \times \exp[-i2\pi\eta t/\Lambda - i\varphi/2 - i\pi/2]\}\end{aligned} \tag{21}$$

and then

$$R_{osc} \approx 1 + 4\sin^2(\varphi/2) - 4\sin(\varphi/2)\sin(2\pi\eta t/\Lambda + \varphi/2). \quad (22)$$

From the above expression, it is possible to study the main features of the oscillation, *i.e.* period, position and amplitude. The oscillation period $\Delta\eta$ is approximately equal to Λ/t. It is about 49 in the case of GaAs(001) with a boundary at a depth $t = 1000$ Å (Fig. 6). It means that the period is about 25 times larger than the Bragg reflection range $\Delta\eta = 2$. The oscillation exhibits a regular sinusoidal shape. Since $R_{p.c.}$ decreases as $1/(4\eta^2)$ far from the Bragg reflection, the oscillation amplitude decreases as $|\sin(\varphi/2)|/\eta^2$. Maximum and minimum correspond to $2\pi\eta t/\Lambda + \varphi/2 = \pm\pi/2$. Thus their positions directly provide the value of φ. Modifications for the absorbing case are negligible far from the Bragg reflection.

Another interesting feature concerns the XSW above the crystal surface. The position of the XSW antinodes is determined by the phase of $\xi^{(a)}$. If one writes $\xi^{(a)} = |\xi^{(a)}|\exp[i\Psi^{(a)}]\exp(i\varphi)$, the position of the antinodes in vacuum is defined with respect to the reflecting planes in the thin part. $\Psi^{(a)} = 0$ means that the antinodes are located at distances that are a multiple of the reflecting plane spacing. We will call this position the reflecting plane position. $\Psi^{(a)} = \pi$ means that the antinodes are shifted by one half of the reflecting plane spacing from the previous position. We will call this position the middle position. Far from the Bragg reflection, it can be seen from (21) that

$$\Psi^{(a)} \approx \Psi + \text{phase of } [1 + 2\sin(\varphi/2) \times \exp(-i2\pi\eta t/\Lambda - i\varphi/2 - i\pi/2)].$$

Ψ is the phase for a single perfect crystal and the second term corresponds to the correction for the oscillating part. $\Psi = \pi$ for $\eta < -1$, decreases to 0 through the Bragg reflection and remains equal to 0 for $\eta > 1$. For $\Psi^{(a)}$, one can distinguish two different behaviours. If $\varphi < \pi/3$ (or $\varphi > 2\pi - \pi/3$), $\Psi^{(a)}$ oscillates around π when $\eta < -1$ and around 0 when $\eta > 1$. The amplitude of the oscillation is $\arcsin[2\sin(\varphi/2)]$ and the period is Λ/t (Fig. 7). This means that the antinode positions move around the middle position for small angles, go to the reflecting plane position through the Bragg reflection and then move around the reflecting plane position for large angles. For $\pi/3 < \varphi < 2\pi - \pi/3$, $\Psi^{(a)}$ decreases from 2π to 0 with period Λ/t (Fig. 7). This means that the antinodes continuously move into the crystal.

4.5. *Relationship between XSW and reflectivity measurements on the thin buried layer*

The XSW analysis of atoms in a thin buried layer can be carried out as usual, with appropriate corrections: (*a*) the transmission term $T(\eta)$ and the anomalous-absorption term $\exp(-t/z_o)$ in the intensity of the X-ray standing waves; (*b*) the oscillating part R_{osc} in the rocking curve. The fluorescence yield $Y(\eta)$ is thus

$$Y \propto T(\eta)\exp(-t/z_o) \times [1 + |\xi^{(+)}|^2 + 2F|\xi^{(+)}|\cos(\Psi - 2\pi P)],$$

where the coherent fraction F and the coherent position P are linked to the distribution of fluorescent atoms $\rho(\mathbf{r})$ by

$$F\exp(i2\pi P) = \frac{\int \rho(\mathbf{r})\exp(i2\pi\mathbf{h}\cdot\mathbf{r})\,d^3\mathbf{r}}{\int \rho(\mathbf{r})\,d^3\mathbf{r}}.$$

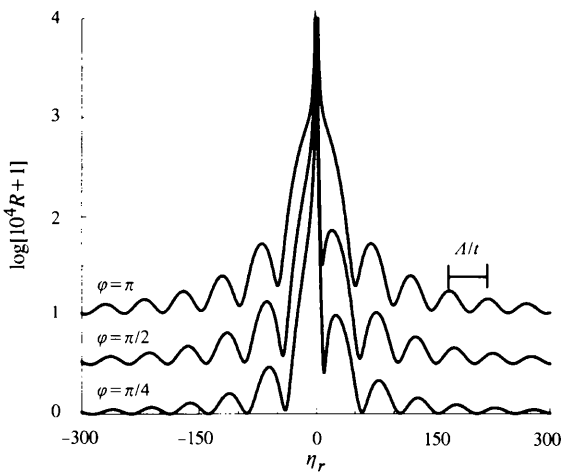

Fig. 6. Reflectivity profiles for $\varphi = \pi/4$, $\pi/2$ and π. Curves in the case of GaAs(001) with a boundary at a depth $t = 1000$ Å, $\lambda = 1.6$ Å and 004 reflection. The absorbing and non-absorbing cases are not distinguishable. The oscillation period is about Λ/t whatever the value of φ. The reflectivity is arbitrarily drawn on a logarithmic scale. The curves are vertically shifted for visibility.

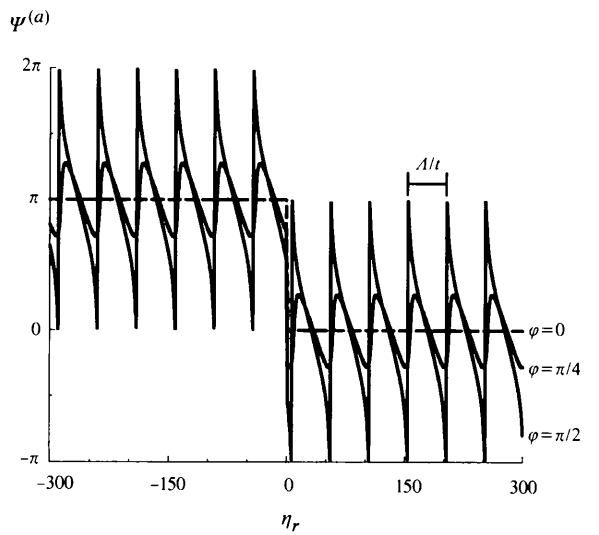

Fig. 7. Phase of the reflected wave in vacuum for $\varphi = \pi/4$, $\pi/2$ and 0 (single perfect crystal). Curves are for the case of GaAs(001) with a boundary at a depth $t = 1000$ Å, $\lambda = 1.6$ Å and 004 reflection.

One may retrieve information about the position of the atoms from the coherent fraction F and the coherent position P. Information about the displacement induced by the buried layer is obtained by the analysis of the reflectivity profile. These parameters are connected and provide complementary information. Let us consider for instance the simplest case of a single buried layer of atoms with similar upper and lower interfaces. The displacement is simply twice the coherent position P: $\varphi = 2\pi(2P)$ modulus 2π (Fig. 8*a*). This relationship is quite general for a symmetric buried layer, *i.e.* with similar upper and lower interfaces.

In this case, the coherent position P is linked to the position of the middle of the buried layer $H/2$:

$$F\exp(i2\pi P) = \frac{\int \rho(\mathbf{r})\exp[i2\pi(\mathbf{h}\cdot\mathbf{r} - H/2)]\,\mathrm{d}^3\mathbf{r}}{\int \rho(\mathbf{r})\,\mathrm{d}^3\mathbf{r}} \times \exp(i2\pi H/2).$$

Since the buried layer considered is symmetric, the ratio in the above expression is real. Depending on the sign of the ratio, P is

$$2\pi P = 2\pi H/2 \quad \text{or} \quad 2\pi H/2 + \pi \,(\text{modulus } 2\pi).$$

The total displacement induced by the buried layer is H:

$$\varphi = 2\pi H = 2\pi(2P)\,(\text{modulus } 2\pi).$$

Thus, $\varphi = 2\pi(2P)$ (modulus 2π) is a criterion of a symmetric buried layer. In practice, atom interdiffusion and surface roughening occur at the interfaces. Thus the buried layer may not be symmetric as schematically drawn in Fig. 8(*b*). This seems to actually happen for real heterostructures studied (Giannini *et al.*, 1993; Takahasi *et al.*, 1995; Boulliard *et al.*, 1997). The relationship between φ and P becomes different from the previous one and the analysis of φ and P allows one to extract the strain parameters of the buried layer.

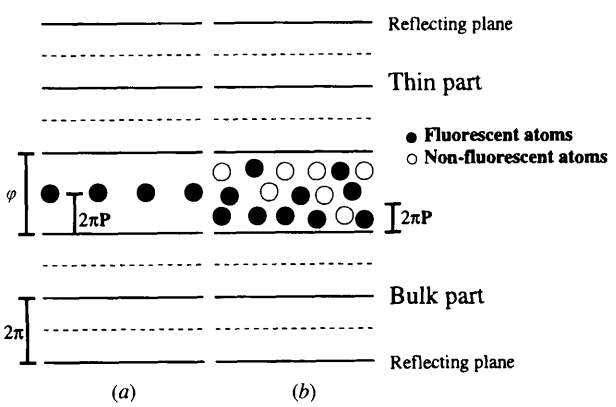

Fig. 8. Relationship between the phase φ and the coherent position P. (*a*) Single and symmetric buried layer: $\varphi = 2\pi(2P)$ modulus 2π. (*b*) Asymmetric buried layer: $\varphi \neq 2\pi(2P)$ modulus 2π.

5. Conclusions

The main characteristic in a crystal containing a thin buried layer is the strong excitation of the backward wavefield in the upper thin part. In the non-absorbing case, the backward wavefield only may be excited for a particular value of η. The strong excitation of the backward wavefield induces an anomalous transmission of the X-rays into the crystal. This phenomenon must be taken into account for the XSW analysis.

It is also shown that, in the case of a symmetric buried layer, the same information on the displacement induced by the buried layer is obtained by the XSW and reflectivity measurements. For an asymmetric buried layer, complementary information is provided by the XSW and reflectivity measurements. This allows an analysis of the strain status in a thin buried layer. Indeed, the problem of the strain in ultrathin layers is not resolved. Generally, the macroscopic elastic model is extended to the case of monolayers. With the XSW and reflectivity measurements, the atom displacements can be determined in the case of monolayers and a more realistic strain model may be considered.

The authors would like to thank Professor Y. Epelboin for kindly providing a careful reading of the paper.

References

Andersen, S. K., Golovchenko, J. A. & Mair, G. (1976). *Phys. Rev. Lett.* **37**, 1141–1145.
Authier, A. (1961). *Bull. Soc. Fr. Minéral. Cristallogr.* **84**, 51–89.
Authier, A. (1986). *Acta Cryst.* A**42**, 414–426.
Authier, A., Gronkowski, J. & Malgrange, C. (1989). *Acta Cryst.* A**45**, 432–441.
Batterman, B. W. (1964). *Phys. Rev. A*, **133**, 759–764.
Batterman, B. W. (1969). *Phys. Rev. Lett.* **22**, 703–705.
Bedzyk, M. J. & Materlik, G. (1985). *Phys. Rev. B*, **32**, 6456–6463.
Bensoussan, S., Malgrange, C. & Sauvage-Simkin, M. (1987). *J. Appl. Cryst.* **22**, 222–229.
Boulliard, J. C., Capelle, B., Gualandris, S., Lifchitz, A., Cibert, J. & Tatarenko, S. (1997). *J. Appl. Phys.* **81**, 1173–1179.
Giannini, C., Tapfer, L., Lagomarsino, S., Boulliard, J. C., Taccoen, A., Capelle, B., Ilg, M., Brandt, O. & Ploog, K. H. (1993). *Phys. Rev. B*, **48**, 11496–11499.
Golovchenko, J. A., Batterman, B. W. & Brown, W. L. (1974). *Phys. Rev. B*, **10**, 4239–4243.
Golovchenko, J. A., Patel, J. R., Kaplan, D. R., Cowan, P. L. & Bedzyk, M. J. (1982). *Phys. Rev. Lett.* **49**, 560–563.
Gronkowski, J. (1991). In *Physics Reports*, Vol. 206. Amsterdam: North Holland.
Hertel, N., Materlik, G. & Zegenhagen, J. (1985). *Z. Phys.* B**58**, 199–204.
Kohn, V. G. & Kovalchuk, M. V. (1981). *Phys. Status Solidi A*, **64**, 359–366.
Kruglov, M. V., Shchemelev, V. N. & Kareva, G. G. (1978). *Phys. Status Solidi A*, **46**, 343–350.

Materlik, G. & Zegenhagen, J. (1984). *Phys. Lett.* A**104**, 47–50.

Taccoen, A., Malgrange, C., Zheng, Y., Boulliard, J. C. & Capelle, B. (1994). *Acta Cryst.* A**50**, 497–503.

Takahasi, M., Nakatani, S., Takahashi, T., Zhang, X., Ando, M., Fukatsu, S. & Shiraki, Y. (1995). *Jpn. J. Appl. Phys.* **34**, 2278–2283.

Vandenberg, J. M., Hamm, R. A. & Chu, S. N. G. (1994). *J. Cryst. Growth*, **144**, 9–14.

Woicik, J. C., Pellegrino, J. G., Southworth, S. H., Shaw, P. S., Karlin, B. A., Bouldin, C. E. & Miyano, K. E. (1995). *Phys. Rev. B*, **52**, R2281–R2284.

Zegenhagen, J. (1993). In *Surface Science Reports*, Vol. 18. Amsterdam: North Holland.